Japanese Journal of Applied Physics
Vol. 43, No. 1A/B, 2004, pp. L 85–L 87
©2004 The Japan Society of Applied Physics

Thermally Driven Thin Film Bulk Acoustic Resonator Voltage Controlled Oscillators Integrated with Microheater Elements

Heon-Min LEE[1,2], Hong-Teuk KIM[1], Hyung-Kyu CHOI[1], Hyung-Ki HONG[1], Don-Hee LEE[1], Jae-Young PARK[1], Jong-Uk BU[1] and Euisik YOON[2]

[1] *Devices & Materials Laboratory, LG Electronics Institute of Technology, 16 Woomyeon-dong, Secho-gu, Seoul 137-724, Korea*
[2] *Department of Electrical Engineering & Computer Science, KAIST, 373-1 Guseong-dong, Yusong-gu, Daejeon 305-701, Korea*

(Received October 14, 2003; accepted November 7, 2003; published December 26, 2003)

In this letter, we report on thermally driven thin film bulk acoustic resonator (TFBAR) voltage-controlled oscillators (VCOs) integrated with a microheater element. The oscillation frequency of TFBAR VCOs is controlled by applying different power (or bias voltage) to the microheaters implemented on the TFBAR membrane. The TFBARs with the microheater elements are fabricated by Si bulk micromachining technology. The series feedback schematic TFBAR VCO has an oscillation frequency of 3.566 GHz, an output power of −21 dBm, and a phase noise of −110 dBc/Hz at an offset frequency of 100 kHz. The measured frequency controllability and the measured temperature coefficient of resistance (TCR) of the heater element are 3.19 MHz/V and 0.24%/°C, respectively, with a resistance of 88.1 Ω at room temperature. [DOI: 10.1143/JJAP.43.L85]

KEYWORDS: TFBAR, VCO, AlN, microheater, bulk micromachining, MEMS

In wireless communication systems, there are increasing demands for voltage-controlled oscillators (VCOs) with a wide tuning range and low phase noise in the 1–10 gigahertz frequency ranges. High-quality VCOs with low phase noise require a high-quality (*Q*)-factor LC tank circuit, but the *Q* factors of conventional on-chip varactors are not adequate.[1–3] Although variable capacitors fabricated using micro-electro-mechanical system (MEMS) technology have been proposed for the off-chip LC tank elements, the *Q* factors of the off-chip MEMS variable capacitors[4–6] are not much higher than those of the on-chip varactors. In recent years, thin film bulk acoustic resonator (TFBARs) have drawn much attraction for use as oscillators that require high-*Q*-factor resonant components with smaller size, lighter weight, and higher performance,[7–9] however, there have been difficulties in controlling the resonant frequencies of the TFBARs by adjusting bias voltage. In this letter, we propose a thermally driven frequency-controllable (or tunable) TFBARs integrated with microheaters as a resonator tank circuit element for VCOs. The resonant frequency of the TFBARs is controlled by applying different power (or applied voltage) to the microheaters implemented on the TFBAR membrane.

The TFBARs made of piezoelectric aluminum nitride (AlN) thin films with microheaters are fabricated using Si bulk micromachining technology. The TFBAR resonant frequencies are highly dependent on the total thickness of the layers contributing to the bulk acoustic resonances, which are made up of a low-stress Si_3N_{4-x} membrane, a Mo bottom electrode on a thin Ti adhesion layer, a piezoelectric AlN thin film, and a Mo top electrode. Figure 1 shows a schematic of the proposed bulk micromachined TFBAR with a microheater element. This microheater element is fabricated on the membrane by the same process used for the formation of the bottom electrode. The detailed fabrication steps are as follows. First, 1.2-μm-thick low-stress Si_3N_{4-x} was deposited on the double side of a 430-μm-thick double-side-polished Si (100) substrate by low pressure chemical vapor deposition (LPCVD). Second, a 200-nm-thick highly (111)-textured Mo/Ti bottom electrode was deposited by RF magnetron sputtering, and patterned by conventional photolithography technique, and then etched using a magnetically enhanced reactive ion etcher (MERIE). The 10-nm-thick Ti layer was inserted to improve the adhesion between Si_3N_{4-x} and Mo. The highly (111)-textured Mo is essential to obtain the highly (002)-textured AlN thin films. The rocking curve of the (111)-textured Mo bottom electrode is 2.3°. Third, the 1.25-μm-thick AlN thin film was deposited, patterned, and etched. The AlN thin film is used as the piezoelectric material in TFBARs and is deposited by reactive RF magnetron sputtering. The base vacuum pressure was kept below 1×10^{-7} mTorr and very pure Ar and N_2 with 99.999% purity were flowed to avoid oxygen contamination to the AlN thin films. The AlN thin films have a highly preferred *c*-axis (002) orientation with a 1.8° rocking curve in the case of 1.3 μm thickness. The AlN thin film was etched mainly by MERIE and finally by wet phosphoric acid at a temperature of 95°C. Fourth, the 250-nm-thick Mo was deposited, patterned, and etched. Finally, the bottom side of Si_3N_{4-x} was opened and the Si (100) was bulk micromachined by wet KOH solution at a temperature of 95°C. The successfully fabricated bulk micromachined TFBAR with an embedded microheater element is shown in Fig. 2.

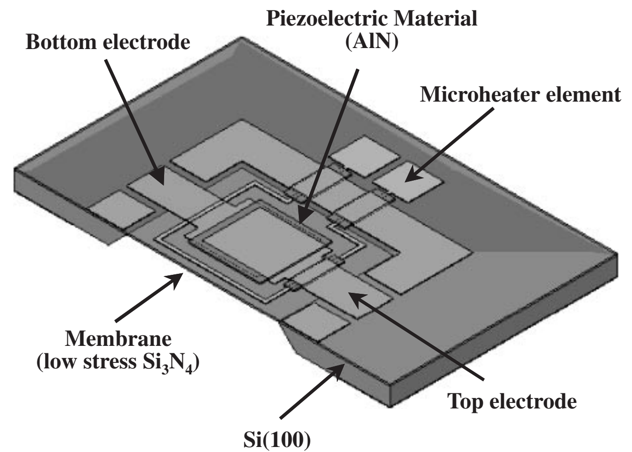

Fig. 1. Schematic of the proposed bulk micromachined TFBAR with a microheater element.

Figure 3 shows the measured scattering parameter S22 and S21 of the TFBAR with a size of $240 \times 240\,\mu m^2$ and it

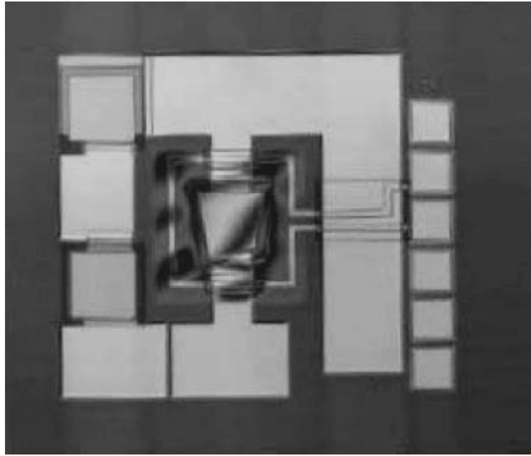

Fig. 2. Photomicrograph of a TFBAR with a microheater element.

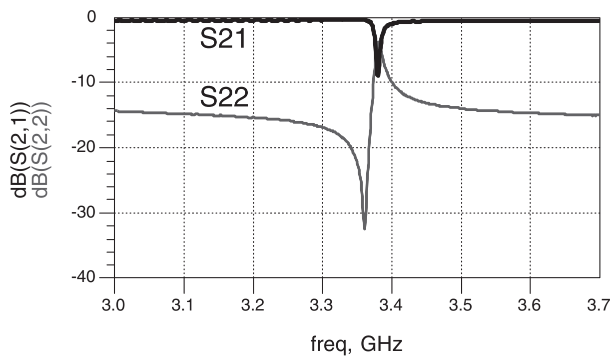

Fig. 3. Measured scattering parameter S22 and S21 of the fabricated resonator with a size of $240 \times 240\,\mu\text{m}^2$.

displays excellent resonant characteristics. The S22 and S21 were measured with a HP8510C network analyzer and a Cascade GSG (ground-signal-ground) probe. The measured electric characteristics are modeled based on the lumped element modified Butterworth-Van Dyke (MBVD) model.[10] The calculated Q factor of 950 based on the MBVD model corresponds well to the Q factor calculated from the measured S22 according to eq. (1). The Q factor of the TFBAR is much higher than that of conventional varactors and the MEMS-based variable capacitors.

$$Q = \frac{2 \times f_r}{\delta f_{3db}} \tag{1}$$

In eq. (1), f_r is the resonant frequency and δf_{3db} is the peak width at half maximum of S22 from the series resonant frequency. The effective piezoelectric coupling constant ($k_{eff}{}^2$) in the resonator and the measured bandwidth are 0.084 and 65 MHz, respectively. $k_{eff}{}^2$ in the bulk micromachined membrane structure is much larger than that in the solidly mounted bulk acoustic resonator (SMR) structure, because the acoustic energy loss in the freestanding membrane is lower than that in the acoustic reflector of the SMR. As the temperature of the TFBAR membrane increases using a microheater, the resonant frequency of TFBAR decreases. Therefore, it is possible to control (or tune) the oscillation frequency of TFBAR VCOs by applying different power (or applied voltage) to the microheaters implemented on the TFBAR membrane. From eq. (2), it is assumed that the decrease in TFBAR resonant frequency is due to the contraction of the AlN thin film sandwiched by the top Mo and the bottom Mo.

$$f_r = \frac{1}{4 \times t} \times \sqrt{\frac{c}{\rho}} \tag{2}$$

In eq. (2), f_r is the resonant frequency, t is the total thickness of the materials contributing to resonance, c is the material stiffness constant, and ρ is the material density.

Figure 4 shows a schematic of the TFBAR VCO. An infineon silicon bipolar device (BFP420) is used as an active device and TFBAR is used as a high-Q frequency-determining element in the emitter terminal. The immitance on the base terminal is optimally determined to obtain negative resistance and phase shift under oscillation conditions. For minimum phase noise in the TFBAR VCO, harmonic suppression and symmetric wave shape are optimized through nonlinear simulation using advanced design system (ADS).[11] The VCO module shown in Fig. 5 was fabricated on a 0.2-mm-thick PPE (ε_r=3.6) substrate using surface-mount-type chips and 1-mil-bond wires. In Fig. 6, the measured output spectrum of a thermally driven TFBAR VCO shows an oscillation frequency of 3.566 GHz and an

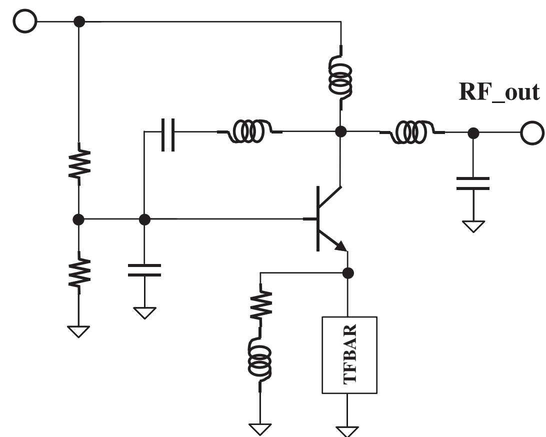

Fig. 4. Series feedback VCO schematic using a TFBAR.

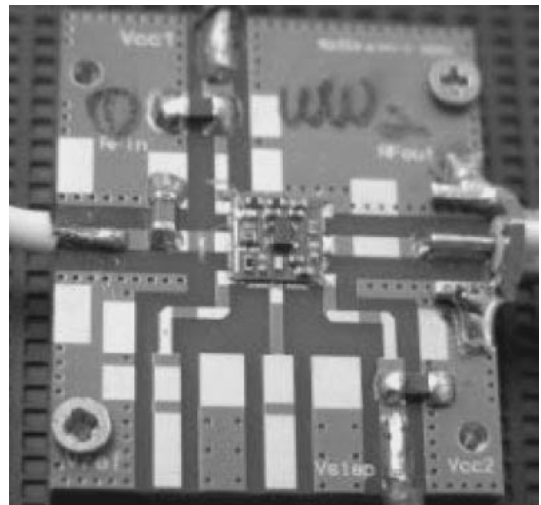

Fig. 5. Photograph of a thermally driven TFBAR VCO module oscillating at 3.566 GHz.

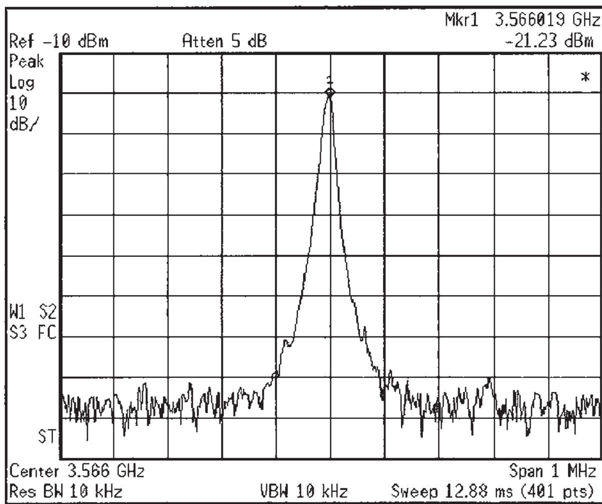

Fig. 6. Measured output spectrum of a thermally driven TFBAR VCO.

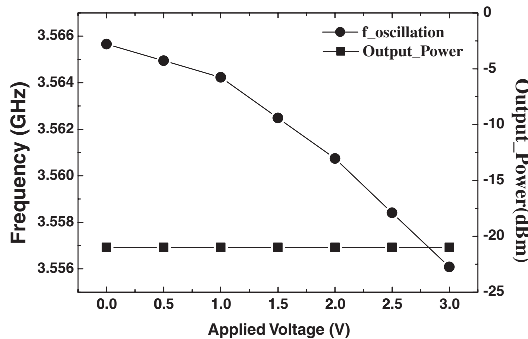

Fig. 7. Oscillation frequency and output power as a function of applied voltage.

output power of -21 dBm at a supply voltage of 2.5 V and a current of 10 mA. From this measured output spectrum, the phase noise is calculated to be -110 dBc/Hz at an offset frequency of 100 kHz. As shown in Fig. 7, the oscillation frequencies of the VCOs are decreased as the applied voltage is increased. The output power has no dependence on the TFBAR membrane temperature. The oscillation frequency was stabilized in 5 ms, after the applied voltage was increased by 0.5 V. The measured frequency controllability and the frequency control range are 3.19 MHz/V and 30 MHz, respectively. Figure 8 shows that the temperature of the TFBAR membrane is linearly dependent on the applied voltage to the microheater. The measured TCR of the heater

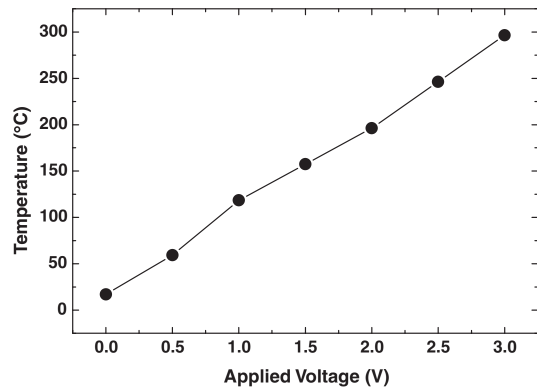

Fig. 8. Membrane temperature of the TFBAR with a microheater element as a function of applied voltage.

element is 0.24%/°C with a resistance of 88.1 Ω at room temperature. The temperature of the heater element and the heating power at the applied voltage of 3 V are 296°C and 74 mW, respectively.

In conclusion, we demonstrated thermally driven TFBAR VCOs integrated with microheater elements. The TFBARs for VCOs are fabricated by Si bulk micromachining technology. In our experiments, it is shown that the resonant frequency of the TFBAR can be thermally controlled with an integrated microheater element. The series feedback TFBAR VCOs with microheater elements have a phase noise of -110 dBc/Hz at an offset frequency of 100 kHz. The frequency control range of 30 MHz and the power consumption of 74 mW at the applied voltage of 3 V are suitable for wireless communication systems.

1) J. Craninckx and M. Steyaert: VLSI Circuit Symp. Tech. Dig. (1996) p. 30.
2) B. Razavi: IEEE ISSCC Tech. Dig. (1997) p. 388.
3) L. Dauphinee, M. Copeland and P. Schvan: IEEE ISSCC Tech. Dig. (1998) p. 224.
4) D. Young and B. Boser: IEEE Solid-State Sensors Actuator Workshop Dig. (1996) p. 86.
5) A. Dec and K. Suyama: Electron. Lett. **33** (1997) 922.
6) A. Dec: IEEE Trans. Microwave Theory & Tech. **48** (2000) 1943.
7) J. M. Rabaey, J. Ammer, T. Karalar, S. Li, B. Otis, M. Sheets and T. Tuan: IEEE ISSCC Tech. Dig. (2002) p. 200.
8) M. Dubious and P. Muralt: Appl. Phys. Lett. **74** (1999) 3032.
9) R. Ruby, P. Bradley, J. D. Larson III, Y. Oshmyansky and D. Figueredo: IEEE ISSCC Tech. Dig. (2001) p. 120.
10) J. D. Larson III, P. Bradley, S. Wartenberg and R. Ruby: IEEE Ultrason. Symp. Dig. **1** (2000) 863.
11) A. Hajimiri and T. H. Lee: IEEE J. Solid-State Circuits **33** (1998) 179.